Chemical and mechanical stability of BCZY-GDC membranes for hydrogen separation

Elisa Mercadelli[a], Angela Gondolini[a]*, Matteo Ardit[b], Giuseppe Cruciani[b], Cesare Melandri[a], Sonia Escolástico[c], José M. Serra[c], Alessandra Sanson[a]

[a] National Council of Research, Institute of Science and Technology for Ceramics, (CNR-ISTEC), Via Granarolo 64, 48018, Faenza, Italy

[b] Department of Physics and Earth Sciences, University of Ferrara, Via Saragat 1, 44122 Ferrara, Italy

[c] Instituto de Tecnología Química (Universitat Politècnica de València-Consejo Superior de Investigaciones Cientifícas), Av. Los Naranjos s/n, E-46022 Valencia, Spain

* Corresponding author: angela.gondolini@istec.cnr.it, Tel.: +39 0546699743, fax: +390546 46381

Keywords Ceramic composite; Hardness; Flexural strength; Aging; Operating Atmosphere

Abstract

This work investigates, for the first time, the hydrogen permeation of $BaCe_{0.65}Zr_{0.20}Y_{0.15}O_{3-\delta}$-$Ce_{0.8}Gd_{0.2}O_{2-\delta}$ (BCZY-GDC) asymmetric membranes for 100 h, using wet 15% CO_2 in Ar as sweep gas. In the same frame, ex-situ aging tests were performed for 100 h exposure at 750°C in different atmospheres (H_2, CO_2, H_2+CO_2), to evaluate the phase, microstructure, and mechanical long-term stability of this system. The thermal aging in H_2-atmosphere leads to lower flexural strength caused by a microstructure embrittlement of the BCZY-GDC asymmetric membrane, due to chemical expansion/contraction of the GDC cell after the aging cycle. Indeed, micro-cracking of GDC grains, that decreases the composite hardness, is observed in symmetric (pressed pellet) membranes. The aging in CO_2 causes a slightly increase in flexural strength values due to the formation of sub-micrometric Zr-doped ceria-$BaCO_3$ phases at the expense of the perovskite, strengthening the membrane microstructure. Higher hardness values related to the emerging of $BaCO_3$ islands on the symmetric membrane surface were also recorded. In H_2+CO_2 atmosphere (real testing condition), the membrane shows a slight decrease in flexural strength and hardness while no evident morphological or structural changes (except the $BaCO_3$ formation in traces) were observed. This study highlights that promising and stable hydrogen permeation flux values (0.08 mL min^{-1} cm^{-2}) can be recorded using the asymmetric configuration for 100 h, using wet 15% CO_2 in Ar as sweep gas. Neither structural nor morphological modification of the membrane were detected after the testing.

Graphical abstract

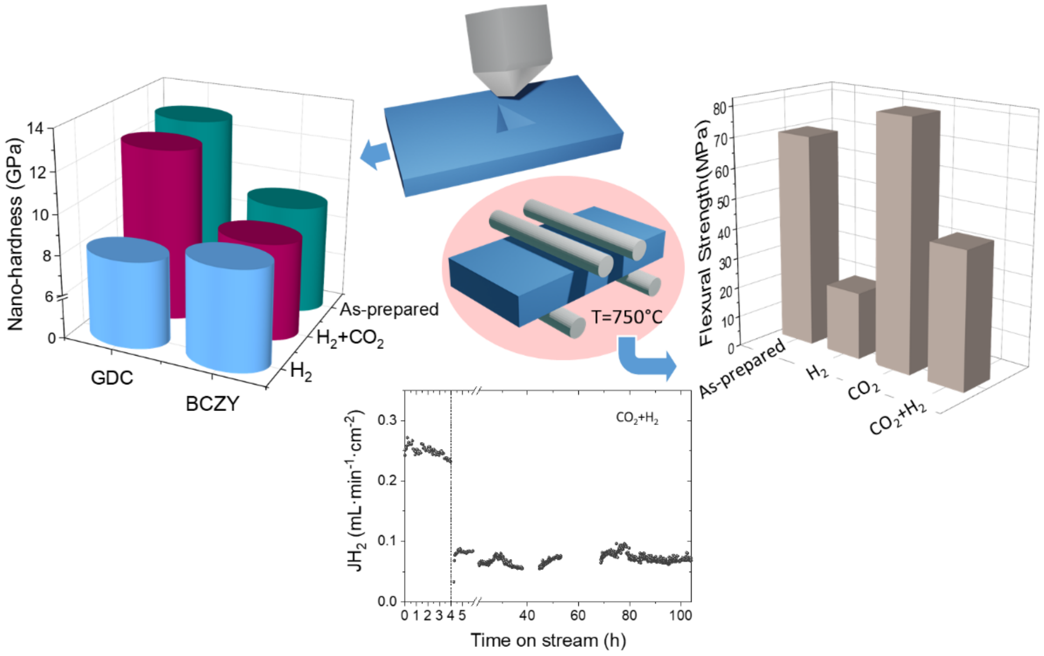

1. Introduction

The European Commission has recently presented the new "European Green Deal", outlining the main policy initiatives for reaching net-zero global warming emissions by 2050 [1]. In this context, hydrogen is confirmed to be a key instrument for meeting the Green Deal objectives, among the others, i) supplying clean, affordable and secure energy, and ii) achieving a carbon neutral, clean and circular economy.

In this direction, the development of innovative hydrogen separation technologies, and more specifically ceramic proton-conducting membranes, is widely recognized to be an important scientific challenge to replace the conventional expensive cryogenic distillation methods in a wide range of application fields, such as fossil fuel processing, production of ammonia and metallurgy engineering, advanced chemical reactors, water-gas shift implants and methane reforming, pure H_2 production, etc.[2–6].

Mixed-conducting ceramic-ceramic composite membranes, based on the combination of a proton conducting perovskite with a suitable ceramic electron conductor, has received increasing attention [7–13] for their capability to separate hydrogen at high temperature (500-1000°C) with 100% selectivity, high chemical and thermal stability and their intrinsic lower cost respect to the Pd – based counterparts. These characteristics make Mixed Proton-Electron Conductor ceramics (MPEC) promising candidates for their easy integration into membrane reactors or pre-existent plants.

Among the MPEC ceramic membranes investigated so far, dense $BaCe_{0.65}Zr_{0.20}Y_{0.15}O_{3-\delta}$-$Ce_{0.8}Gd_{0.2}O_{2-\delta}$ (BCZY-GDC) composites have shown encouraging performances in terms of H_2 permeation, reaching H_2 flux values up to 0.68 mL min^{-1} cm^{-2} at 750 °C [14], robustness towards CO_2 [15] and acceptable stability under 700 ppm of H_2S containing atmospheres in operating conditions [16].

In this regard, a lot of work has been done to assess i) the compatibility issues of the perovskite and fluorite phases during the processing steps [17], ii) the process parameters to obtain planar BCZY-GDC asymmetric membranes [18–21], iii) the structural evolution of the composite under real working conditions, i.e. high temperatures and harsh reducing conditions [22]. The latter highlights that BCZY-GDC composite does not show, in operando, evidence of chemical reaction between the phases under dry and wet H_2 in the 300-800°C temperature range. Moreover, a synergic effect was observed for the two phases showing a tendency to reach similar volume expansion in operating conditions, strengthening the real application potential of this kind of membranes.

However, to effectively approach the market, together with high hydrogen fluxes and thermochemical stability, the ceramic membranes must ensure long-term reliable performances under operating conditions, among which the mechanical aspect plays a crucial role and must be considered as well [23]. Structural, morphological, and chemical alterations may in fact occur after long time exposure at high temperatures under operational atmospheres (that could contain CO_2, CO, H_2, H_2O, hydrocarbons and H_2S) detrimentally affecting hydrogen permeability and long-term chemical and mechanical stability.

In addition, from the mechanical point of view, it must be considered that the membrane thickness must be reduced as much as possible to enhance the H_2 permeation. A practical way is to fabricate an asymmetrical architecture in which the active membrane layer is anchored to a porous mechanically stable support [24]. Thus, the mechanical reliability of such a bi-layer composite design clearly depends on mechanical stability and the structural integrity of both the membrane and substrate.

Even if thermomechanical studies and lifetime predictions have been performed in deep for oxygen-conducting ceramic membranes also in asymmetrical configuration [25–27], to the best of our knowledge, very few studies have been conducted onto planar ceramic membranes for hydrogen separation, being the latter focused only onto lanthanide tungstate-based systems [28–31].

For BCZY-GDC-based membranes only one work has been published on the performance in CO_2 environment for the symmetric configuration for 24 hours of operation [15]. The hydrogen permeation rate using 15% CO_2 in Ar as sweep gas, 50% H_2 in He as the feed gas was found to be higher than 0.005 mL min^{-1} cm^{-1}.

This work aims to investigate for the first time the structural, microstructural and mechanical stability of BCZY-GDC composites after 100 h exposure at 750 ºC in different atmospheres: (i) H_2, (ii) CO_2 and (iii) H_2+CO_2 mixture. The composition of the latter was selected mimicking the one of the most common conditions used for permeation tests, i.e. 15 vol% CO_2 in Ar (135 $mL·min^{-1}$) and H_2 (50 $mL·min^{-1}$). Hydrogen permeation of BCZY-GDC asymmetric membrane was also evaluated for 100 h of operation, using wet 15% CO_2 in Ar as sweep gas to assess its long-term performances. Structural stability was studied by X-ray diffraction and TG measurements whereas microstructural properties were studied by SEM. Mechanical properties of the composite before and after the treatments were characterized by three different techniques: 4-pt flexure strength at 750 °C, indentation and nano-indentation at room temperature. To the author best knowledge this is the first time that the mechanical properties of BCZY- GDC systems were investigated in real atmosphere and temperature of operation.

2. Experimental

2.1 Membranes production

BCZY-GDC composite membranes were produced both in asymmetrical and symmetrical configuration as required for each specific characterization/testing technique implemented in this work.

The asymmetric BCZY-GDC membranes were prepared by tape casting. For the porous support, BCZY ($BaCe_{0.65}Zr_{0.20}Y_{0.15}O_{3-\delta}$, Specific Surface Area (SSA) = 5.8 m^2/g, supplied by Marion Technology, France) and GDC powders ($Ce_{0.8}Gd_{0.2}O_{2-\delta}$, SSA = 6.8 m^2/g, supplied by FuelCellMaterials, USA) were used as starting material in a ratio equal to 50/50 vol %. Rice Starch (Fluka, Germany), with average particle size of 5-6 µm was used as sacrificial pore forming agent. The amount of starch added to the slurry was the 53 vol % respect to the ceramic powder as previously optimized in [20]. On the other hand, BCZY (SSA = 12.2 m^2/g, supplied by Marion Technology, France) and GDC powders in a ratio equal to 50/50 vol % were used to produce the dense membrane layer. An amount of 1 wt% ZnO (Sigma Aldrich) respect to the powders was used as sintering aid and directly added into the tape casting suspension. For a detailed description of the slurry's composition, preparation and casting parameters, the interested reader is referred to the previous works [18,20].

The green tapes were punched in discs of 24 mm in diameter for the permeation test, while for bending tests, strips of 35 x 8 mm^2 size were cut. An uniaxial warm press (55 °C applying a pressure of 0.7 bar) was used to laminate the porous support with the active membrane layer to produce the asymmetrical BCZY-GDC structure.

The bilayers were finally debinded and sintered at 1550 °C for 4 h. A 50/50 vol% mixture of BCZY-GDC was used as source of barium during sintering following the experimental set-up already reported in [19]. The resulting asymmetric membranes were 0.65 ± 0.5 mm thick.

The symmetric BCZY-GDC membranes were prepared by die pressing. The 50/50 vol% mixture of BCZY-GDC powders with 1 wt % ZnO was ball milled in ethanol (99 %, Sigma Aldrich) for 2 h, dried at 50 °C and finally sieved at 75 µm. The resulting powder was uniaxially pressed in a Ø = 12 mm die at 750 Kg/cm^2 and isostatically pressed at 3000 bar. The green pellets were finally sintered at 1550 °C for 4 h, with the same sintering set-up used for the tape cast membranes. All the sintered pellets reached relative density values of 98.4 ± 0.8 %.

2.2 Aging treatments

To investigate the influence of the operating atmosphere on the thermomechanical stability of the BCZY-GDC membranes, both symmetrical and asymmetrical membranes were aged at 750°C for 100h in different atmospheres: H_2, CO_2 and H_2+CO_2. In the case of symmetrical membranes, one surface side of each pellet was polished down to 0.25 µm finish before the aging treatment to perform the nano-indentation tests. All the samples were placed onto ad-hoc perforated alumina setters (Keralpor 99, Kerafol) to guarantee the maximum exposure to the aging atmosphere.

The aging treatment in reducing atmosphere was performed in a tubular furnace (Nabertherm, Germany), setting an Ar/H_2 (4 vol%) flow rate equal to 50 L h^{-1}. On the other hand, samples were aged in a saturated CO_2 atmosphere in a conventional furnace setting a pure CO_2 flow equal to 50 L h^{-1}. The third aging treatment was performed in a tubular reactor under a stream composed by 15 vol% CO_2 in Ar (135 mL·min^{-1}) and H_2 (50 mL·min^{-1}). This gas composition was selected to be comparable with the one used during the permeation test (same gas flows).

2.3 Characterizations

The 4-pt flexural strength of the as-prepared and thermally aged asymmetric membranes was measured at 750 °C in Ar flow (3.5 L min^{-1}) using the furnace HTTF 974 (Severn Fornaces). The tape cast bars with dimensions about $25.5 \times 5.5 \times 0.6$ mm^3 (length by width by thickness, respectively) were tested using a universal screw-driven load frame for mechanical testing (Instron mod. 1195, Instron). An alumina flexural jig with upper and lower span of 10 and 20 mm, respectively was used, while the specimens were broken with a crosshead speed of 0.5 mm min^{-1}. Before applying the load during testing at high temperature, a dwell of 15 min was set to reach thermal equilibrium. For each set of samples, at least 5 bars were tested.

Vickers microhardness (HV) was measured on the polished surface of the as-prepared and thermally aged symmetric BCZY-GDC membranes (pellets), with a load of 4.9 N, using a Innovatest Falcon 505 (Innovatest, The Netherlands) indenter. The value provided (expressed in HV) is the average of 10 indentations.

Nano-hardness of BCZY and GDC grains was investigated using a commercial nanoindenter (MTS mod. XP, MTS Systems Corporation, Oak Ridge, TN, USA) equipped with a Berkovich diamond tip. The tests were performed using polished samples (as prepared and thermally aged BCZY-GDC composite pellets) with a peak load of 5 mN. The nano-indenter was continuously loaded with a strain rate target of 0.05 s^{-1} up to the peak load and immediately unloaded with no holding time. For each sample 90 indentations, spaced at 5 μm, were made. Hardness (H) was calculated according to a computational procedure included in the nanoindenter software TestWorks™ ver. 4.06 A, which is based on the model of Oliver and Pharr (2004). The software automatically subtracted both the machine compliance and thermal drift. The nano-hardness values are expressed in GPa.

Prior to X-Ray Powder Diffraction (XRPD) analyses, as-prepared and thermally aged asymmetric membranes were ground in an agate mortar with a pestle. Data collection was performed at room-temperature (RT) on a Bruker D8 Advance Da Vinci diffractometer working in Bragg-Brentano geometry, and equipped with a Cu-anode X-ray tube, Ni-filter to suppress Cu Kβ component, and a LynxEye XE silicon strip detector (angular range of the detector window size = 2.585° 2θ) set to discriminate Cu Kα1,2 radiation. The powder of each sample was placed over a monocrystalline Si low background sample holder and scanned in a continuous mode from 5-135° 2θ with step size of 0.015 ° 2θ and a counting time of 1.5 s per step. To minimize the preferred orientation of crystallites, the sample was spun at 25 rpm to increase crystallite statistics, and a knife perpendicular to the sample was placed at a suitable distance from the sample surface to reduce the air-induced scattering. An additional measurement at RT was performed using the same experimental setup on the bulk BCZY-GDC membrane on both dense and porous side after permeation tests.

Qualitative phase analysis was performed by means of the Bruker AXS EVA software (v.5), while each collected X-ray powder diffraction pattern was Rietveld refined by means of the fundamental-parameter approach (TOPAS v.5.0). All the identified phases were modeled by carrying out multiphase refinements in which only the scale factor, unit-cell parameters, and the crystallite size were varied. The crystallite size was calculated by means of the "integral breadth" based LVol calculation derived from a profile peak convolution in a Lorentzian-type broadening approximation.

Results of the quantitative phases analysis for the bulk BCZY-GDC membrane after permeation tests (Table S1) are deposited as supplemental material.

Thermogravimetric (TG) analysis (STA 449, Netzsch, Selb/Bavaria, Germany) was performed to assess the CO_2 uptake of the asymmetric BCZY-GDC membrane at 750 °C for 100 h. 80 mL min^{-1} of dry CO_2 and 20 mL min^{-1} of dry N_2 were fed during the analysis.

The microstructure of the sintered membranes was investigated by scanning electron microscopy (SEM-FEG, Carl Zeiss Sigma NTS GmbH, Oberkochen, Germany), embedding the cross sections under vacuum in epoxy resin and then polishing them down to 0.25 µm finish. For the asymmetrical membranes, the porosity amount of the support as well as the residual porosity and thickness of the dense active layer were calculated via image analysis of the SEM micrographs using ImageJ software (Java, ORACLE, Redwood City, California). The chemical composition before and after the aging treatment was assessed by semi-quantitative analysis with an EDS probe (EDS, X-Act, INCA Energy 300, Oxford Instruments, Abingdon, UK).

Hydrogen permeation stability of the as-prepared asymmetric BCZY-GDC membrane was evaluated for 100 h by using as sweep side an atmosphere composed by 15 vol% CO_2 in Ar (135 $mL\cdot min^{-1}$) at 750 ºC. A mixture of 1:1 H_2-He (100 $mL\cdot min^{-1}$) was used as feed gas. Both streams were humidified at room temperature (3 % H_2O). Sweep gas was fed on the porous substrate whereas feed gas was introduced on the dense membrane layer. The H_2 content in the permeate side was analyzed using micro-GC Varian CP-4900 equipped with Molsieve5A and PoraPlot-Q glass capillary modules. Sealing was accomplished using a silver-based alloy ring.

The surface of the dense membrane and the porous support were catalytically activated with Pt. A Pt catalytic layer was screen-printed on the dense membrane side whereas the porous support was infiltrated with a 0.15 M solution of Pt (tetraammineplatinum (II) nitrate). Subsequently, sample was dried at 150 ºC and calcined at 750 ºC.

3. Results and Discussion

3.1 Flexural tests of asymmetric BCZY-GDC membranes

The influence of the aging atmosphere on the thermomechanical stability of the asymmetric BCZY-GDC membranes was investigated through 4-pt flexure tests at the selected working temperature of 750°C. The results are illustrated in Figure 1.

Collected data show that the flexural strength values are in the same order of magnitude of dense (symmetrical) lanthanum tungstate-based membranes tested at high temperatures [30], i.e., around 70 MPa for untreated samples. The nature of the aging atmosphere strongly influences the mechanical performances of the present membranes as can be observed in Figure 1. In particular, the membranes exposed to H_2 atmosphere registers a collapse of the flexural strength values while the membranes aged in CO_2 show a slightly higher flexural strength compared to the ones collected for the as-prepared samples. Lastly, the thermal treatment in H_2+CO_2 atmosphere leads to strength values that are in between to those registered for the two single atmospheres (H_2 and CO_2). This result indicates that for the asymmetric membrane there is a balancing effect between the increase of the flexural strength due to the CO_2 treatment and the embrittlement of the structure given by H_2.

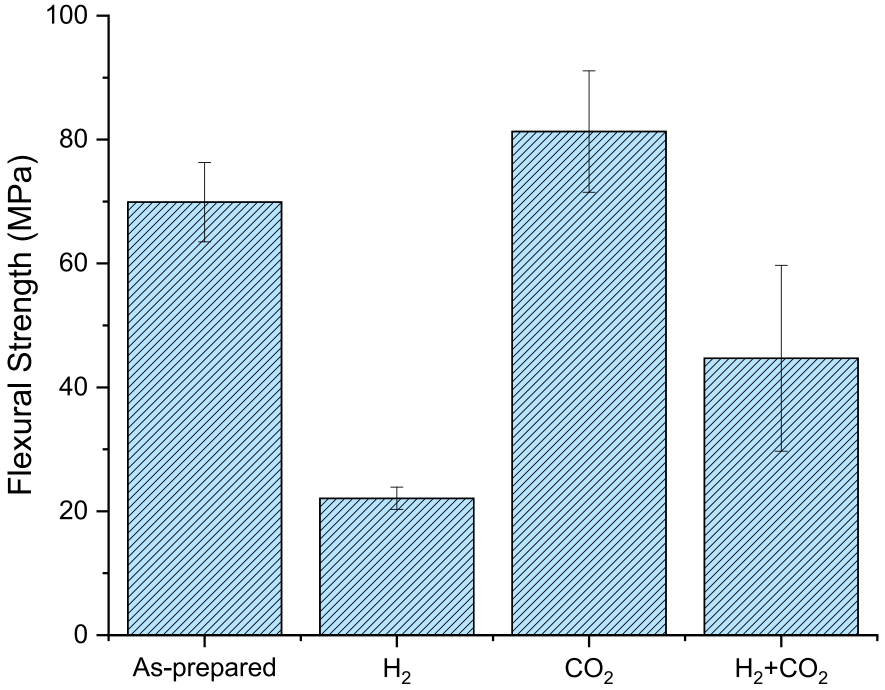

Figure 1 Flexural strength values of asymmetric BCZY-GDC membranes registered at 750°C after thermal aging at 750°C for 100 h in different atmospheres: as-prepared, H_2, CO_2 and H_2+CO_2.

3.2 Microstructural and morphological characterization of asymmetric membranes

To understand the as-described mechanical behaviour, the influence of the operating atmosphere on the microstructural and morphological properties of the asymmetric BCZY-GDC membranes were investigated through XRD and SEM-EDS analyses.

Rietveld refinement plots for collected XRPD patterns of the as-prepared and aged membranes are reported in Figure 2, while the results of the quantitative phases analysis are shown in Table 1 and as in-set graphs inside the corresponding plot. Refinement of the as-prepared BCZY-GDC membrane confirms the presence of both GDC and BCZY phases with phase fractions equal to 51.7 ± 0.1 % GDC and 48.3 ± 0.1 % BCZY in weight. The resulting phase fraction is very closed to the nominal one, where a 50-50 vol.% corresponding to 54-46 wt% GDC-BCZY phase proportion is expected, thus confirming that the constituting phases are preserved during the production process. The phase fraction ratio of perovskite- and fluorite-type crystal structures is also maintained when the membrane is exposed for 100 h at 750°C in H_2 and H_2+CO_2 atmosphere (Table 1), although in the latter condition the partial reaction between the BCZY and CO_2 leads to the formation of detectable traces of witherite $BaCO_3$ (< LoQ value). Nevertheless, a remarkable compositional variation is detected when the asymmetric membrane is aged in pure CO_2 atmosphere. Unlike the GDC fluorite phase, which is not affected by thermal aging treatments, the BCZY perovskite tends to completely decompose under CO_2 atmosphere (2.4 wt% of residual perovskite is detected) in favour of an almost equal amount of witherite $BaCO_3$ (23.4 wt%) and Zr-doped ceria ZDC (24.2 wt%). The chemical stability against the CO_2 of BCZY-based compounds is in fact a well-known critical issue [32].

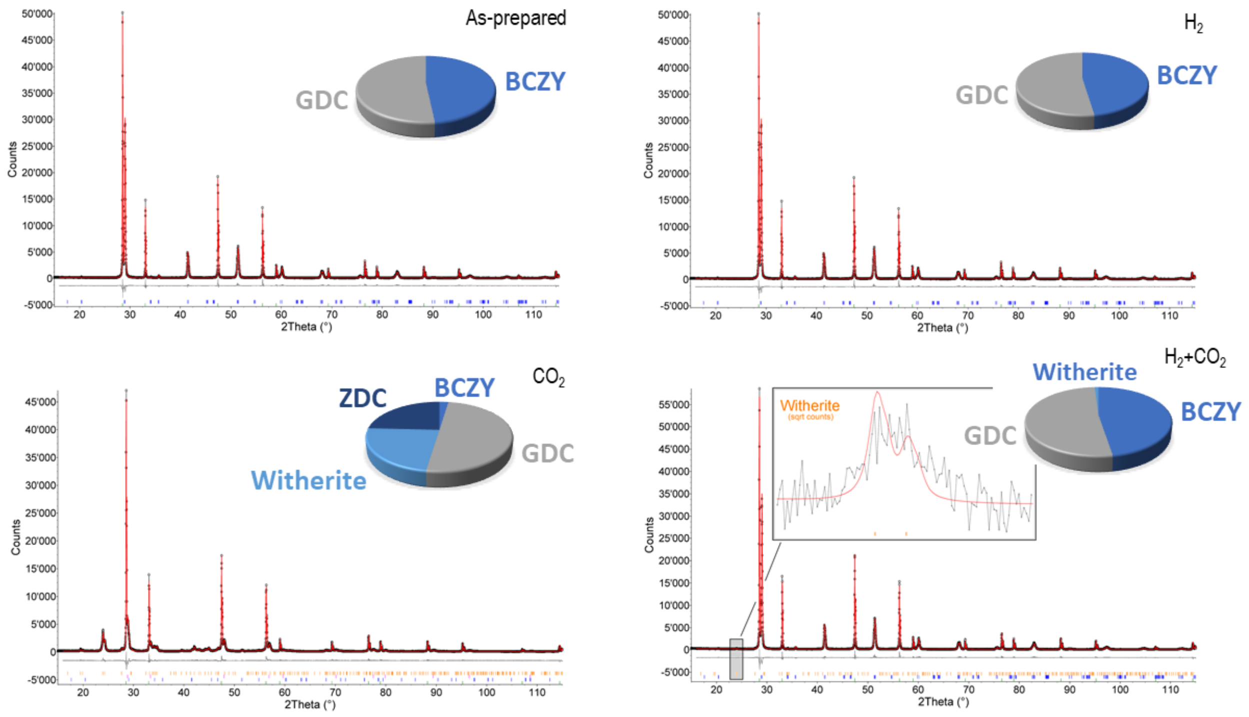

Figure 2 Rietveld refinement plots of the XRPD patterns collected at RT for investigated asymmetric BCZY-GDC membranes (i.e. as prepared and aged at 750 °C for 100 h in different atmospheres). The experimental profile is represented by black dots, the continuous red line is the calculated pattern, while the lower grey curve is the difference between calculated and observed intensities. Vertical ticks mark the position of phase reflections.

Table 1. Refinement agreement factors, quantitative phase analysis, unit-cell parameters, and crystallite size with their standard deviations for the BCZY-GDC as-prepared membrane and after treatments at 750 °C for 100 h in different aging atmospheres (*i.e.*, H_2, CO_2, and H_2+CO_2). BCZY, GDC, and ZDC stand for $Ba(Ce_{0.65}Zr_{0.2}Y_{0.15})O_{2.925}$ with perovskite structure and, $(Ce_{0.8}Gd_{0.2})O_{1.9}$ and $(Ce_{1-x}Zr_x)O_2$ (ZDC) with fluorite-type structure, respectively.

	Phase	**R_{Bragg}**	**Wt%**	**s.g.**	***a*** (Å)	***b*** (Å)	***c*** (Å)	***V*** ($Å^3$)	**Crystallite size (nm)**	**R_{wp}**
As-prepared	BCZY	0.043	48.3(1)	*Imma*	6.1538(2)	8.6861(2)	6.1819(1)	330.43(1)	198(10)	0.085
	GDC	0.040	51.7(1)	*Fm-3m*	5.4206(2)	–	–	159.27(1)	225(11)	
H_2	BCZY	0.049	47.6(1)	*Imma*	6.1538(2)	8.6848(2)	6.1816(1)	330.38(1)	243(19)	0.096
	GDC	0.040	52.4(1)	*Fm-3m*	5.4209(2)	–	–	159.30(1)	220(15)	
CO_2	BCZY	0.016	2.4(1)	*Imma*	–	–	–	–	32(7)	0.092
	GDC	0.039	50.0(3)	*Fm-3m*	5.4201(2)	–	–	159.22(1)	215(5)	
	witherite	0.029	23.4(2)	*Pmcn*	5.3053(4)	8.9109(6)	6.4490(5)	304.87(4)	32(7)	
	ZDC	0.039	24.2(5)	*Fm-3m*	5.3647(1)	–	–	154.40(1)	32(7)	
H_2+CO_2	BCZY	0.052	47.9(1)	*Imma*	6.1543(2)	8.6863(2)	6.1813(1)	330.44(1)	148(6)	0.086
	GDC	0.043	52.1(1)	*Fm-3m*	5.4204(2)	–	–	159.25(1)	216(9)	
	witherite	–	< 1.	*Pmcn*	–	–	–	–	–	

NOTE: since the formation of witherite and ZDC phases takes place at the expenses of the BCZY phase, the crystallite size for those phases has been constrained to be the same.

The $BaCO_3$ formation, resulting from X-ray diffraction analysis, is corroborated by the data registered as weight variation for the asymmetric membranes before and after the aging treatment in CO_2 and H_2+CO_2 atmosphere (Table 2). Furthermore, the thermogravimetric curve (Figure 3) registered for the asymmetric membrane under a CO_2-N_2 flux (80 vol% of CO_2) suggests similar values of CO_2 uptake, highlighting the highest rate of carbonation reaction after 1000 min (16 h) at 750°C, reaching a weight stabilization after 5000 min (83 h).

Table 2 Weight variation registered for the asymmetric BCZY-GDC membranes.

Aging atmosphere	**CO_2 uptake (wt%)**	**$BaCO_3$ (wt%)**
CO_2	5.3 ± 0.1	23.9 ± 0.6
H_2+CO_2	0.09 ± 0.04	0.4 ± 0.2

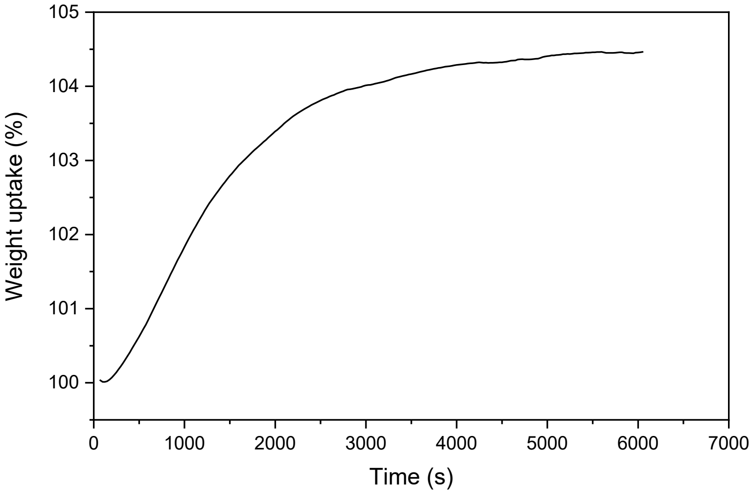

Figure 3 Thermogravimetric curve registered at 750 °C for an asymmetric BCZY-GDC membrane under CO_2 (80 mL min^{-1}) - N_2 (20 mL min^{-1}) flux.

Further evidence on the effects of thermal aging treatments undergone by the BCZY-GDC membranes can be inferred from the variation of unit-cell parameters and crystallite size of detected phases (Table 1). While the GDC phase is unaffected from treatments in different atmospheres (i.e. lattice parameters vary within uncertainties, and the same crystallite size is retained), the BCZY with perovskite structure seems to be more reactive at the different external conditions. The latter phase, that keeps almost unchanged after the treatment in H_2, shows a first evidence of phase transformation after the aging in H_2+CO_2 atmosphere. Although volumetric changes are not observed, a 25% crystallite size decreasing (i.e. from ~200 nm of the as-prepared sample to ~150 nm) occurred. Nevertheless, as previously observed, the prolonged aging in CO_2 atmosphere promotes the formation of witherite and Zr-doped ceria at BCZY perovskite expense. The new phases as well as the residual BCZY are characterized by a crystallite size which is one seventh (i.e. about 30 nm) of that of the BCZY perovskite phase in the as-prepared membrane. The formation of these secondary phases with higher packing density in respect to the primary BCZY-GDC phases and constituted by crystals in the nanometric range is responsible of the higher flexural strength registered for the CO_2-aged membrane (Figure 1).

Summarizing, the data collected from X-ray analysis performed onto asymmetric membranes suggest that: i) the BCZY phase tends to completely reacts with CO_2 at 750 °C, in saturated CO_2 atmosphere, forming $BaCO_3$ and Zr-doped ceria phases constituted by nanometric-size crystals; ii) no remarkable evidence of changes onto membranes aged in H_2; iii) the aging treatment in H_2+CO_2 atmosphere leads to the formation of < 1 wt% $BaCO_3$ after 100 h, and to a BCZY crystallite size decrease of about 25%.

To further investigate the effect of the operating atmosphere onto the morphological properties of the asymmetric membranes, SEM-EDS analyses were performed before and after each aging treatment. The micrographs of the polished cross sections of the asymmetric membranes aged at 750°C for 100 h in H_2, CO_2 or H_2+CO_2 are reported in Figure 4. The as-prepared membrane is constituted by a highly porous (44 ± 2%) support and a 16 ± 1 µm thick active layer with closed porosity < 5 % (Figure 4a). Moreover, SEM analysis of the backscattered electron (BSE) evidences a homogeneous distribution of light grey areas related to the GDC phase as well as dark areas attributed to BCZY. The peculiar topography of the polished cross sections shown in Figure 5 is the result of the hardness contrast between the harder GDC (light grey) and the softer BCZY (dark) as already observed in [14].

When the membrane is aged in H_2 atmosphere (Figure 4b), no apparent morphological differences can be observed. However, some cracks across the active membrane layer were detected after sample embedding/polishing. This indicates that structural changes occur in the membrane during the thermal cycle under H_2 at 750 °C for 100 h and back to ambient (oxidant) atmosphere, favouring the embrittlement of the membrane and thus lowering its fracture strength. In fact, even if no cell parameters variation was registered after this aging treatment due to re-oxidation phenomena in ambient atmosphere (Table 1), it is widely demonstrated from in-situ synchrotron XRD analyses in reducing conditions [22,33] that doped-CeO_2 materials show a significant non-linear expansion of the cubic cell due to the reduction of Ce^{4+} to Ce^{3+}, predominant at $T > 600°C$.

On the other hand, a morphological transformation was clearly detected for the sample aged in CO_2 (Figure S1). The dark grey areas related to BCZY are in fact replaced by sub-micrometric grains (either dark or light), mainly distinguishable on the top surface of the dense active layer and throughout the porous support section. This phenomenon is reasonably associated to the decomposition of the perovskite phase into $BaCO_3$ (dark grains) and ZDC (light grains) as previously demonstrated by XRD analyses.

Finally, no morphological changes can be appreciated when the membrane is subjected to a thermal cycle at 750 °C for 100 h in H_2+CO_2 atmosphere (Figure 4d).

Focused electron beam EDS profiles of Ba, Gd and C elements (Figure S2) were also recorded on the polished fractures of the active membrane layer to assess the stability towards CO_2 and to confirm the distribution of BCZY and GDC. EDS profiles for Ba and Gd demonstrate the homogeneous distribution of the fluorite and perovskite phases for the membranes investigated. On the other hand, EDS profile of carbon confirms the lack of carbonated species in the as-prepared,

H_2- and H_2+CO_2-aged samples, while a detectable carbon concentration profile is visible for the membrane aged in CO_2, especially in the first 1.0 µm starting from the upper surface.

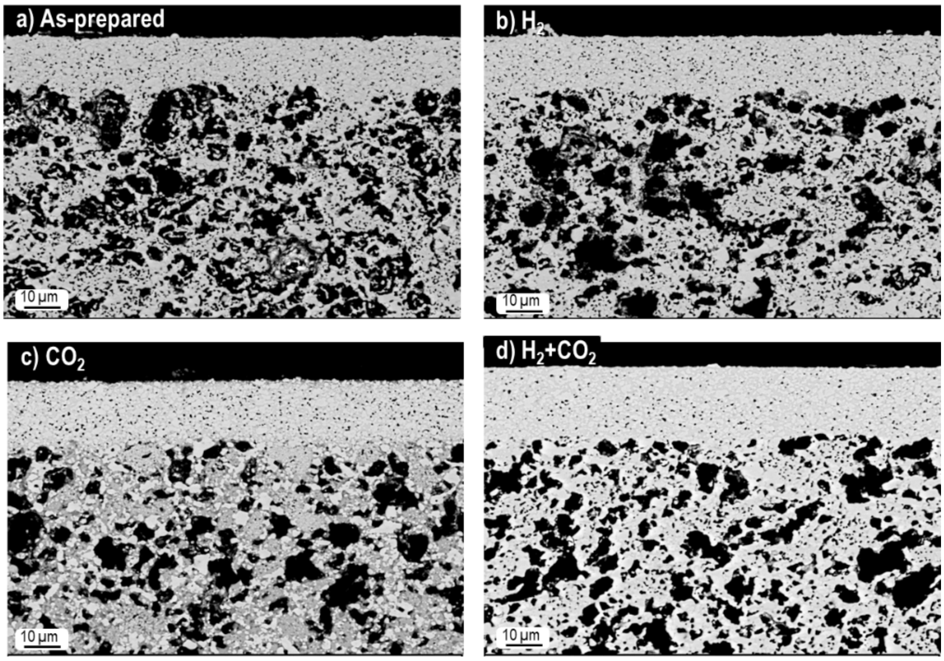

Figure 4 BSE-SEM micrographs of the polished cross sections of the asymmetric membranes aged at 750 °C for 100 h in different atmospheres: as-prepared (a), H_2 (b), CO_2 (c), H_2+CO_2 (d).

Finally, the influence of the aging treatment at 750°C for 100 h in different atmospheres on the dense active layer surface morphology of the asymmetric membranes is shown in Figure 5. According to the previously reported results, no detectable surface modification is registered for the membrane treated in H_2 atmosphere that show the same round-shape grains microstructure. On the other hand, morphological alterations occur when the membranes are aged in H_2+CO_2 and CO_2 atmospheres. Even if the former preserves the grain boundary microstructure (with respect to as-prepared sample), small amounts of impurity phase (i.e. $BaCO_3$, in accordance with the Rietveld refinement results) in the nanometric range are clearly distinguished at the grains surface. A similar surface modification has been already observed for BCZY-based ceramic pellets after CO_2 exposure at 700 °C for 10 h [34]. Indeed Cheng et al. showed a similar surface microstructure for a

$BaCe_{0.8}Y_{0.2}O_{3-\delta}$-$Ce_{0.8}Y_{0.2}O_{2-\delta}$/$BaCe_{0.8}Y_{0.2}O_{3-\delta}$-Ni hollow fiber membrane after stability test at 850 °C (125 h), using 7% CO_2−N_2 as the sweep gas, even if no discussion was given about the nano-sized impurities formation localized at the membrane surface [35]. On the contrary, a significant change in the microstructure of the BCZY-GDC dense surface after CO_2 treatment (Figure 5c) is observed due to the presence of sharp-cornered grains microstructure in respect to the ones reported in Figure 5 a) and b). The grains of this microstructure are present continuously on the upper surface of the CO_2 aged membrane and they are attributed to a witherite coating formed by the CO_2-BCZY reaction.

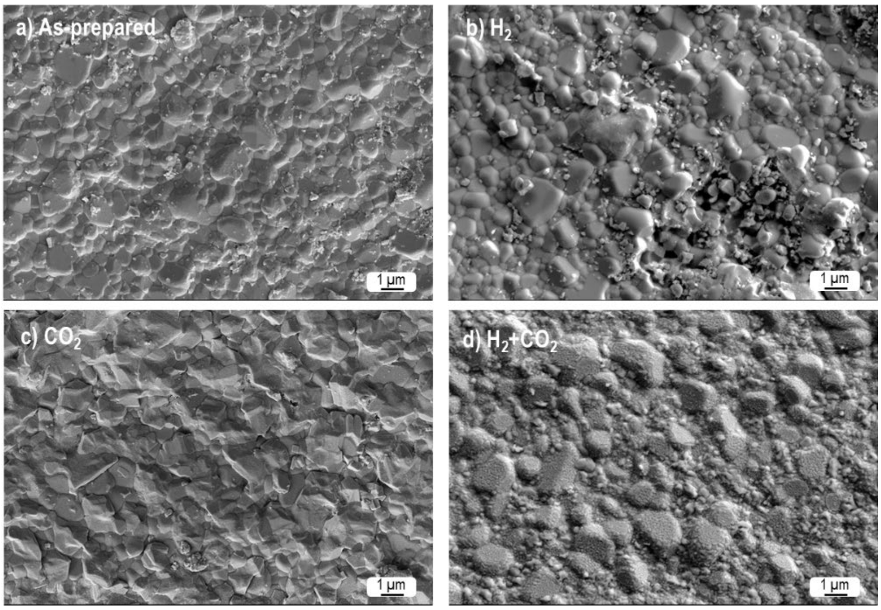

Figure 5 SEM micrographs of the dense active layer surface of the asymmetric membranes aged at 750 °C for 100 h in different atmospheres: as-prepared (a), H_2 (b), CO_2 (c), H_2+CO_2 (d).

Thereby, according to the XRD data coupled with SEM results, the mechanical behaviour of asymmetric BCZY-GDC membranes can be explained as follow: i) the exposure of the membrane to H_2-atmosphere (at 750°C x 100 h) leads to a lower flexural strength caused by a general embrittlement of the structure probably consequence of chemical expansion/contraction of the GDC cell after the aging cycle; it has been already noticed [36,37] that the reduction of Ce^{4+} to Ce^{3+} provokes an expansion of lattice resulting in mechanical strains that could affect the lifespan of this material; ii) the aging in CO_2 atmosphere causes an increase in flexural strength values due to the formation, especially in the porous support, of ZDC-$BaCO_3$ sub-micrometric phases at the expense of the perovskite, strengthening the membrane microstructure; iii) the membrane aged in the operating H_2+CO_2 atmosphere, simulating the one used during practical permeation test, shows only a slight decrease in flexural strength because no evident morphological or structural changes (except the $BaCO_3$ formation in trace amount) were observed.

3.3 Indentation/nano-indentation tests of symmetric BCZY-GDC membranes and their morphological characterization

To further investigate the mechanical behaviour of BCZY-GDC composite, indentation and nanoindentation tests were performed onto symmetric membranes (pressed pellets) before and after the same aging treatments used for their corresponding asymmetric structures.

The hardness values reported in Figure 6 show a trend comparable to the one registered for the flexural strength of the asymmetric membranes (Figure 1) apart from the values registered in H_2+CO_2 atmosphere. Similarly, while a thermal aging in H_2 atmosphere causes a hardness decrease, the exposure to CO_2 leads to hardness increase. On the other hand, hardness values of symmetric membrane aged in H_2+CO_2 atmosphere remain almost constant indicating a negligible influence of the H_2+CO_2 atmosphere on the hardness values. This result, apparently in contrast with the trend observed for flexural strength (Figure 1), is nonetheless roughly a balance between the values registered after aging in H_2 and CO_2 as observed for the flexural strengths of the asymmetric structures.

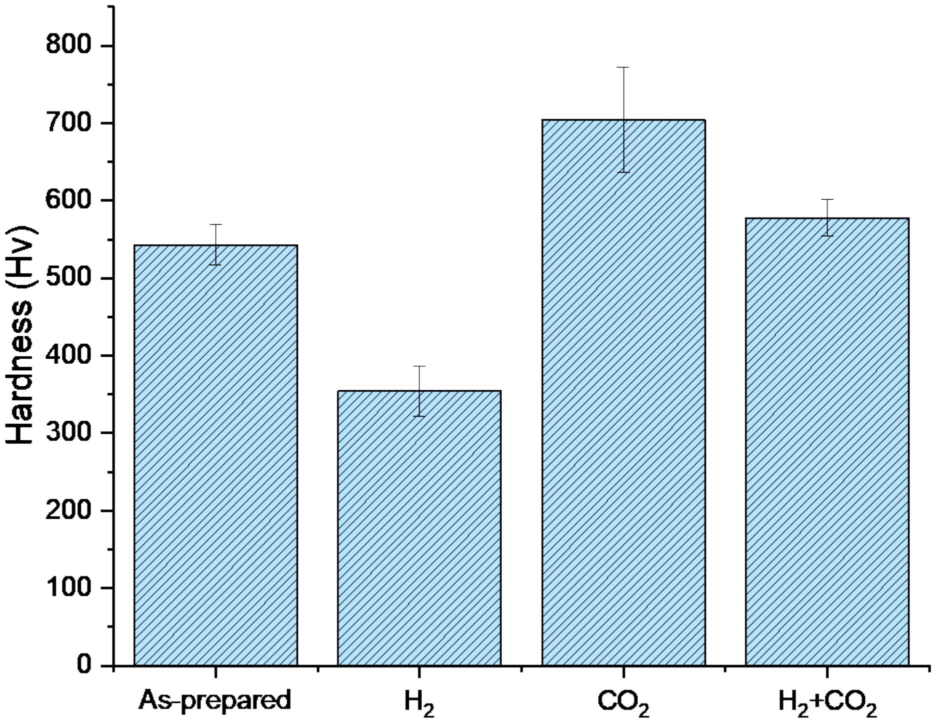

Figure 6 Hardness values measured by indentation tests of symmetric BCZY-GDC membranes (pellets) registered after thermal aging at 750 °C for 100 h in different atmospheres (as-prepared, H_2, CO_2 and H_2+CO_2).

To better understand this behaviour, SEM analyses were performed onto the upper surfaces (indented side) (Figure 7), and onto polished fracture surfaces (Figure 8) of the as-prepared and thermally aged BCZY-GDC pellets (symmetric membranes). It is evident in this case that the operating atmosphere strongly affects the microstructures of the membranes.

As shown in Figure 7b and 8b, the H_2 atmosphere leads to the formation of micro cracks, concentrated in the GDC grains (lighter ones). This phenomenon is caused by the abovementioned chemical expansion/contraction of the GDC cell after the aging cycle. Differently from the asymmetric structure, the membranes in form of pellets are constituted by a less porous microstructure with larger BCZY and GDC grains, because of the different production process (i.e. tape casting and die pressing respectively). For these reasons, the effects of volume cell variations are more pronounced and detectable at the microscopic level. However, it is worth to highlight that the extended cracks observed in Fig. 7b are detectable only onto the aged-surface level. On the contrary, microcracks are well-confined inside the GDC grains for the bulk of the pellet.

When the BCZY-GDC pellets are exposed to CO_2 atmosphere, the formation/emerging of $BaCO_3$ "islands" of sharped-cornered grain microstructure is observed at the upper surface of the membrane (Figure 7c). This is in contrast with what observed on the dense active layer surface of the asymmetric membrane for which a uniform coating of $BaCO_3$ was clearly observed (Figure 5c). Moreover, the fracture surface reported in Figures 8c and S3a shows that the BCZY-CO_2 reaction occurs only at the first 3.8 ± 0.6 µm in thickness, as clearly determined by C-, Ba-, Gd-EDS profiles (Figure S3a). This confirms the key-role of the membrane architecture: while the carbonation reaction drastically affects the whole asymmetric membrane due to the open porous structure, the BCZY-GDC pellets are only aged at the surface level. The latter is confirmed by the calculated 0.0165 ± 0.0007 wt% of CO_2 uptake corresponding to the formation of 0.07 ± 0.003 wt% of $BaCO_3$.

Finally, as observed for the asymmetric structure, the aging in H_2+CO_2 also causes the formation of larger $BaCO_3$ (micrometric in size) (Figure 7d), that could be seen as the early stage of the $BaCO_3$ "islands" structures formation observed for surface aged in pure CO_2. The cross section of the BCZY-GDC pellet treated in H_2+CO_2 (Figures 8d and S3b) shows no appreciable microstructural variations. Indeed, in this case, no weight variation (i.e. below detection limit) associated to CO_2 uptake was registered for the symmetric membranes before and after the aging treatment.

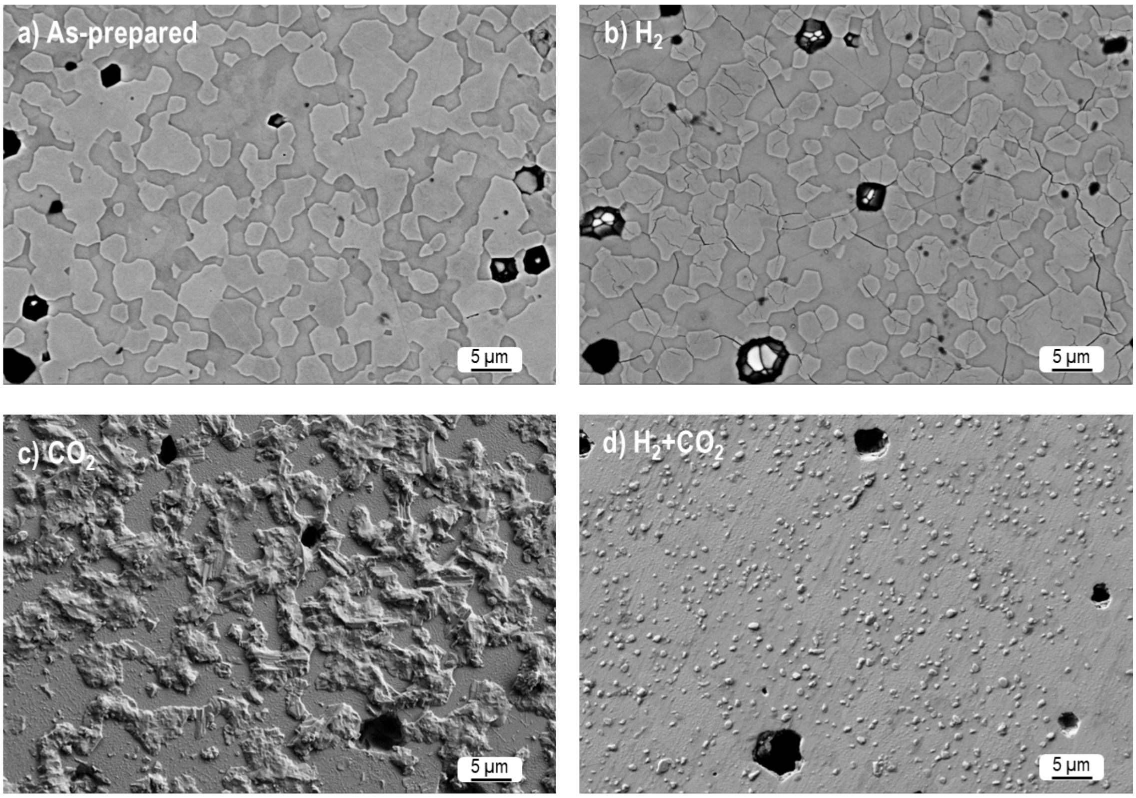

Figure 7 SEM micrographs of the upper surfaces of symmetric BCZY-GDC membranes (pellets) after thermally aged at 750 °C for 100 h in different atmospheres: as-prepared (a), H_2 (b), CO_2 (c), H_2+CO_2 (d).

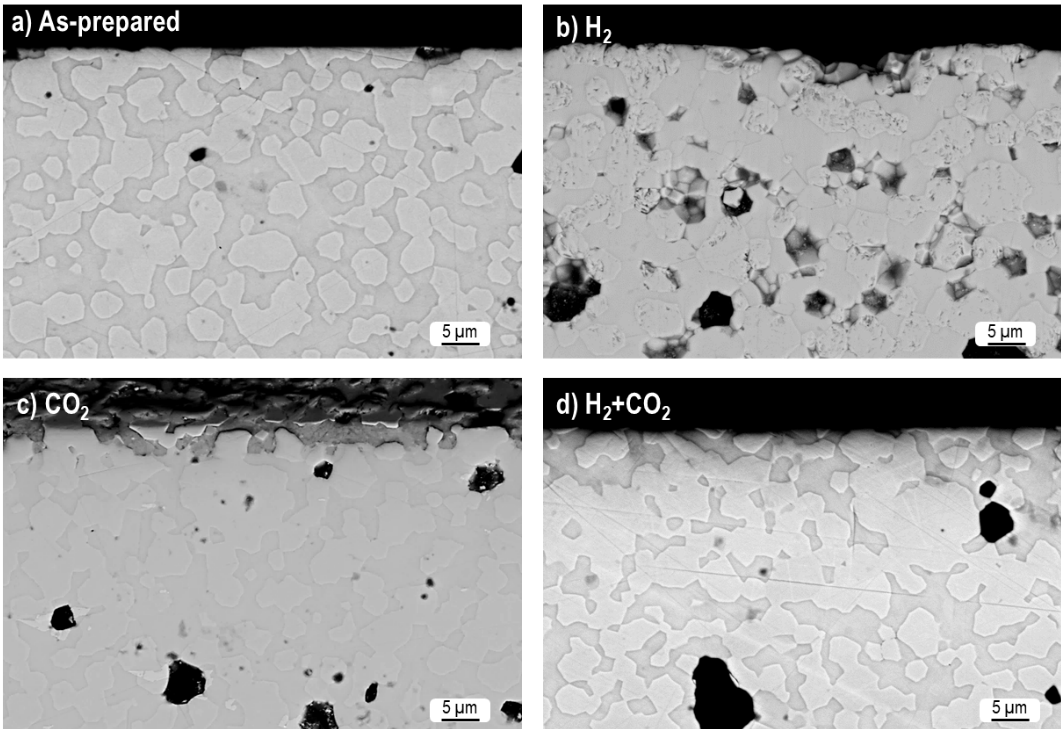

Figure 8 SEM micrographs of the polished fracture surfaces of symmetric BCZY-GDC membranes (pellets) thermally aged at 750 °C for 100 h in different atmospheres: as-prepared (a), H_2 (b), CO_2 (c), H_2+CO_2 (d).

To detect the hardness of the single perovskite and fluorite phases, nanoindentation tests were performed onto the polished surface of BCZY-GDC pellets (Figure 9 a) before and after the thermal aging in different atmospheres. Note that for the sample aged in CO_2 atmosphere, due to the lack of planarity caused by the formation/emerging of $BaCO_3$ “islands”, no reliable results could be registered. As shown in Figure 9b and 9c, load-displacement curves were acquired for both BCZY and GDC phases.

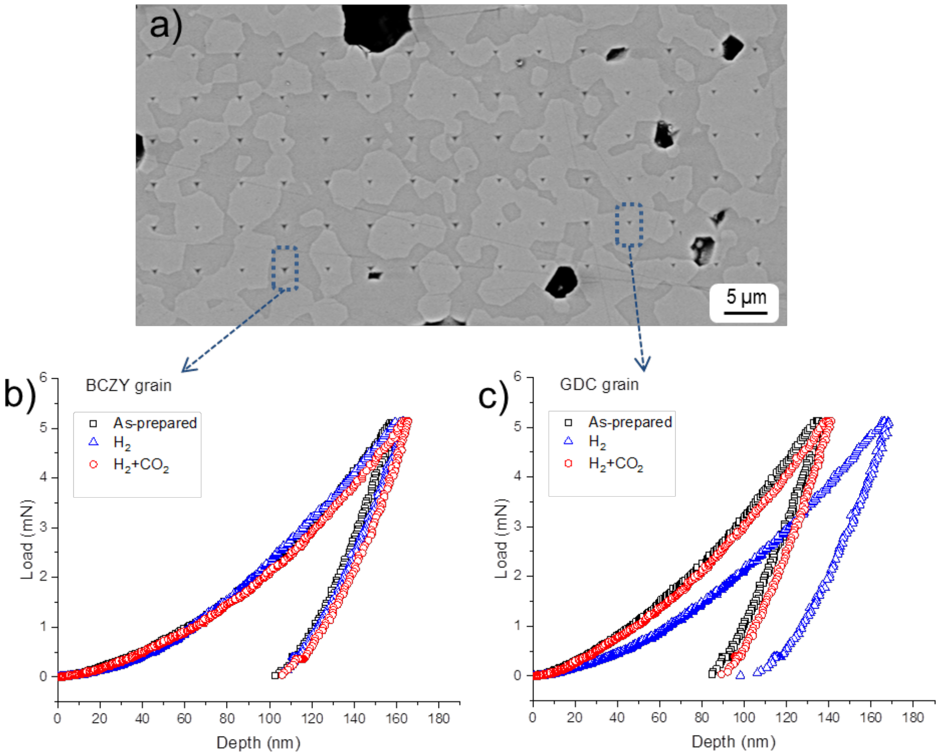

Figure 9 a) BSE-SEM micrograph of the BCZY-GDC membrane (pellet) surface exposed to the aging atmosphere with the corresponding 90 nano-indentations. Load-displacement curves for b) BCZY and c) GDC grains before and after thermal aging at 750 °C for 100 h in H_2 and H_2+CO_2

atmosphere. Note that the load-displacement curves were not registered for membranes aged in CO_2 due to lack of planarity caused by the formation/emerging of $BaCO_3$ "islands" (Figure 8).

The nano-hardness and Young's Modulus values extracted from the load-displacement curves are plotted in Figure 10 a) and b). The as-prepared composite is constituted by GDC and BCZY phases with calculated nano-hardness of 12.8 ± 2.1 GPa and 9.2 ± 1.9 GPa respectively. These data are consistent to the ones reported in previous works [38–40]. When the membrane is exposed to H_2+CO_2, no evident variation in nano-hardness is registered for the BCZY and GDC phases, confirming the hardness results previously described, whereas the thermal aging in H_2 atmosphere strongly affects the GDC nano-hardness. Its decrease is once again associated to the micro-cracking phenomenon already observed through SEM analyses, thus proving the issue associated to cycling treatments in these conditions. The trends registered for the Young's Modulus (Figure 10 b)) are in accordance with the ones showed for nano-hardness.

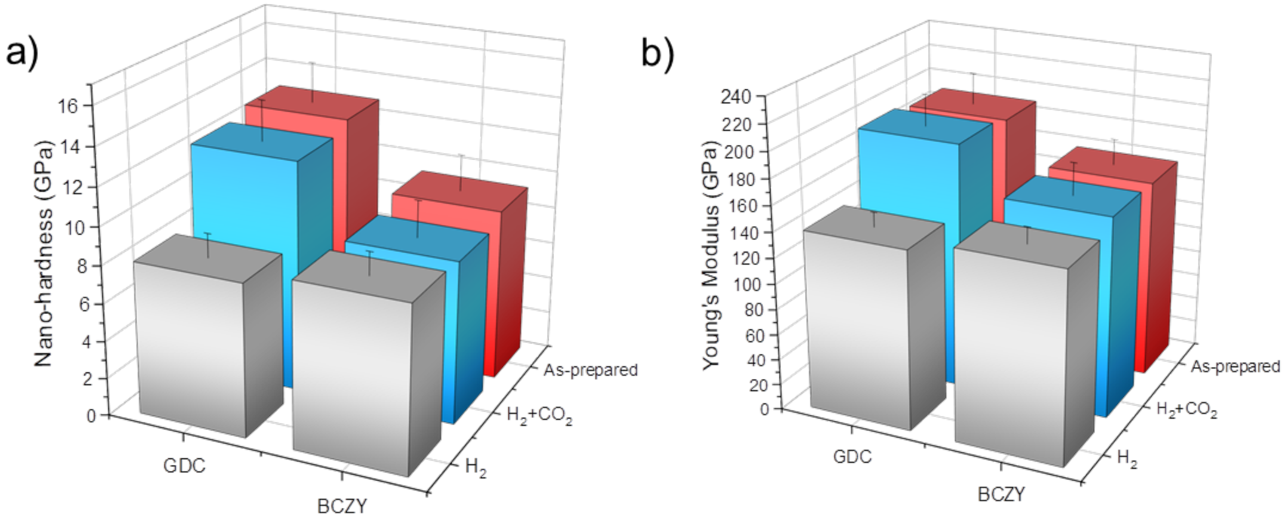

Figure 10 Nano-hardness a) and Young's Modulus values b) determined for each of the two phases constituting the composite membrane (BCZY and GDC) determined through nano-indentation tests onto the pellets surface before and after the aging treatments.

3.4 Hydrogen permeation test and post-mortem analyses.

Hydrogen permeation stability of the as-prepared asymmetric BCZY-GDC membrane, with a dense active layer 18.7 ± 1.2 µm thick, was evaluated for 100 h by using as sweep side an atmosphere composed by 15 vol% CO_2 in Ar (135 $mL \cdot min^{-1}$) at 750 ºC. Sweep gas was fed on the porous substrate side (permeate side), and the H_2/He mixture was fed on the dense membrane layer side.

Figure 11 plots the H_2 permeation values as a function of time on stream. First, the permeation test was carried out for 4 h by using Ar as sweep gas. The sweep gas was then switched to 15 vol% CO_2 in Ar stream. H_2 permeation flux values steeply decrease when CO_2 was added in the sweep gas and then remain stable for 100 h. This decrease agrees with that observed in a previous work for BCZY–GDC bulk membranes [15] and it is ascribed to the CO_2/H_2 competitive adsorption on the membrane surface. This phenomenon was studied in deep by Sato et al. [41] investigating the influence of CO_2-rich flux on the H_2 permeation of Pd-based dense membranes. The permeation calculated at 573 K decreased with the increasing of CO_2 ratio primarily attributed to the formation of carbonous species at the membrane surface. However, these surface species at 673 K, were not produced. For this reason, in our study, the lowering of the permeation flux is attributed to the CO_2 adsorption on the surface sites [42]. This competitive adsorption leads to a reduced H_2 adsorption and subsequent decreasing in hydrogen permeation.

On the other hand, the lower H_2 fluxes as compared with previous studies by using a similar membrane [14] are ascribed to the concentration polarization resistance in the porous substrate as Ar and CO_2 were fed in the porous support side, where molecular diffusion is the predominant transport mechanism, and both gases possess higher kinetic diameter than H_2 and He. Note that small oscillations/scattering observed in the permeation values may be due to the variations in the temperature of the water saturator variations (room temperature).

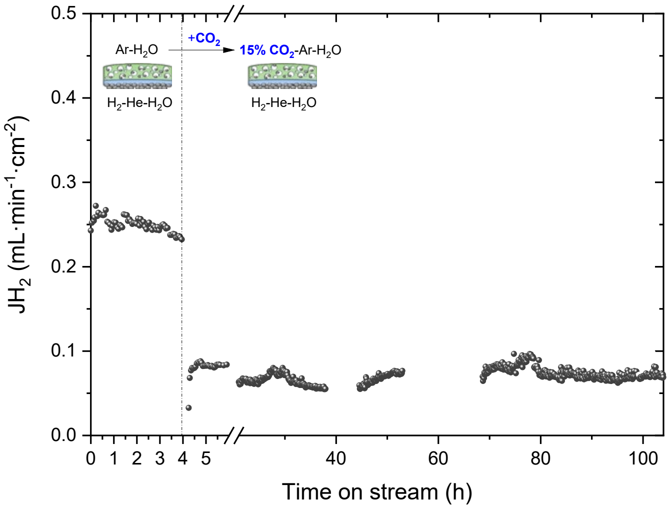

Figure 11 H_2 permeation values as a function of time on stream by using wet Ar and 15 vol% CO_2 in Ar as sweep gas. Line indicates the addition of CO_2 to the sweep.

After permeation measurements using CO_2 in the sweep gas for 100 h, the membranes were investigated through XRD and SEM analyses to assess any morphological and/or compositional modifications.

The XRD plots and Rietveld refinement results shown in Figure 12 and Table S1 respectively, confirm the preservation of the perovskite and fluorite phases, with detectable traces of witherite $BaCO_3$ (< 1 wt%). This is in accordance with the results obtained for the asymmetric membrane aged in H_2+CO_2 atmosphere (for which the aging conditions were selected to mimic the ones the permeation test), previously discussed.

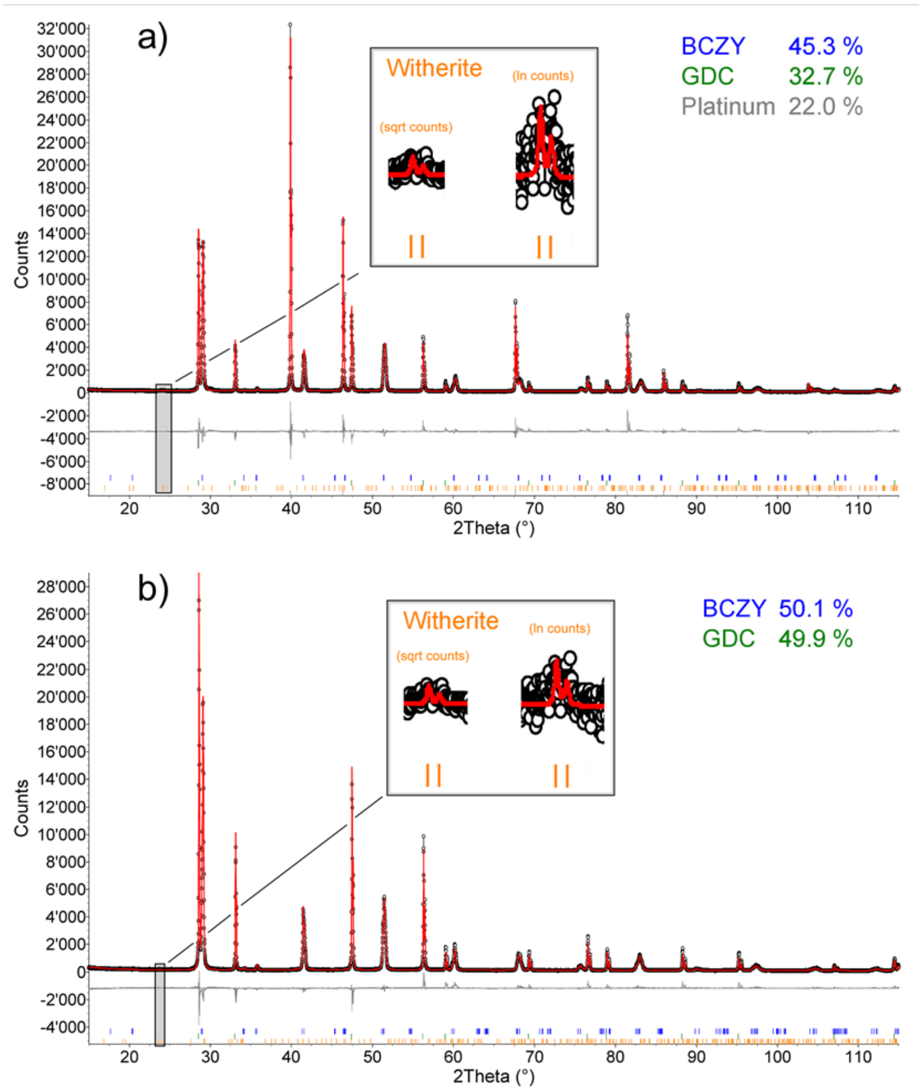

Figure 12 XRD patterns of the BCZY-GDC membrane on both dense (a) and porous (b) sides of the membrane (exposed to feed (a) and sweep stream (b)) after permeation measurements.

Comparing the microstructural characterization of the as-prepared membrane (Figure 4a) with the post-mortem results (Figure 13a and S4b), it is evident that no detectable morphological and compositional alterations occurred during permeation tests.

No cracks were in fact discernible into the fresh cross section of the membrane, while EDS profiles (Figure S4b) for barium and gadolinium demonstrate that the homogeneous distribution of the fluorite and perovskite phases is preserved. On the other hand, EDS profile of carbon (Figure S4a) confirms the lack of detectable carbonated species after the permeation test using CO_2.

Finally, the SEM micrographs of the fresh fracture depicted in Figure S4b show that the Pt nanoparticles maintained their morphology and distribution through the BCZY-GDC porous support.

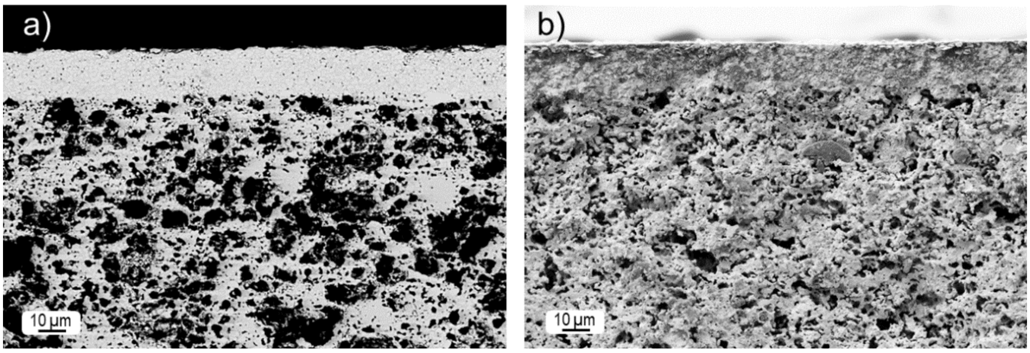

Figure 13 SEM micrographs of the asymmetric BCZY-GDC asymmetric membrane after permeation measurements: a) polished cross section and b) fracture surface.

It is important to notice that the H_2 flux achieved in this work is very promising considering the ones reported in literature (Table 3), especially among the ceramic-ceramic composite membranes. Even if the influence of the CO_2 atmosphere on the hydrogen permeation performances is generally reported, very few information is available concerning the membrane mechanical stability after a prolonged operating condition. Therefore, the results obtained in this work demonstrate the general good stability of these systems under H_2+CO_2 atmosphere, even for long-time operation (100 h) with promising permeation fluxes.

Table 3 Summary of hydrogen performances for membranes tested in CO_2 atmosphere.

Membrane composition	**Architecture**	**Thickness (μm)**	**Temperature (°C)**	**H_2 flux (mL min^{-1} cm^{-2})**	**Feed (a)/sweep (b)**	**Phase and morphology stability**	**Thermo-Mechanical properties**
Ceramic-Metallic composite							
Pd-Y_2O_3-stabilized ZrO_2, 60:40 vol% [43]	Asymmetric planar structure	18	400-500	≈10 for 120 days	(a) 50% H_2, 30% CO_2, 1% CO, 3% H_2O, 16% He, 500 mL min^{-1} (b) N_2 ≈ 500 mL min^{-1}	Not reported	Not reported
Ni-Ba($Zr_{0.1}Ce_{0.7}Y_{0.2}$)-O_{3-d}, 40:60 vol% [44]	Symmetric pellet	266	900	0.35 for 80 h	(a) wet 20% CO_2, 80% H_2-He (40-60) (b) 100 ppm H_2/N_2	Sufficient stability verified by SEM in [45]	Not reported
Ni–$BaZr_{0.1}Ce_{0.7}Y_{0.1}Yb_{0.1}O_{3-\delta}$ (, 40:60 vol% [46]	Symmetric pellet	560	900	0.0625	(a) wet 20% H_2, 60% CO_2, 20% He, 100 mL min^{-1} (b) N_2	$BaCO_3$ formation due to the degradation of Ni–$BaZr_{0.1}Ce_{0.7}Y_{0.1}Yb_{0.1}O_{3-\delta}$.	Not reported
Ni- Ba($Zr_{0.7}Pr_{0.1}Y_{0.2}$)O_3 , 40:60 vol% [47]	Symmetric pellet	400	850	0.008 for 40h	(a) wet 30% CO_2, 70% H_2-He (40-60) (b) Ar 20 mL min^{-1}	Stable verified by XRD and SEM	Little cracks are found in the Ni or Ba($Zr_{0.7}Pr_{0.1}Y_{0.2}$)O_3 surface of particles due to lattice expansion
$Ba_{0.95}Ce_{0.85}Tb_{0.05}Zr_{0.1}O_{3-\delta}$ / Ni-$Ba_{0.95}Ce_{0.85}Tb_{0.05}Zr_{0.1}O_{3-\delta}$ (40-60 wt%) [48]	Asymmetric Hollow fiber	14	800	0.3 for 25 days	(a) 50 vol% H_2/ 50 vol% He, with a flow rate of 80 mL min^{-1} (b)7 vol% of CO_2 in N_2 as sweep gas at flow rate 80 mL min^{-1}).	Stable verified by XRD and SEM	TEC evaluations in air. Sufficient matching
$BaCe_{0.8}Y_{0.2}O_{3-\delta}$ – $Ce_{0.8}Y_{0.2}O_{2-\delta}$ (28.6-71.4 wt%) / $BaCe_{0.8}Y_{0.2}O_{3-\delta}$ – $Ce_{0.8}Y_{0.2}O_{2-\delta}$ (90-10 wt%) [35]	Asymmetric Hollow fiber	17	850	1.34 for 125 h	50 vol% H_2/ 50 vol% He, 100 mL min^{-1} (b) 7% CO_2–N_2, 80 mL min^{-1}	Stable verified by XRD and SEM	TEC evaluations in air reported in [49]. Good thermal expansion matching
Ceramic-ceramic composite							

$SrCe_{0.95}Y_{0.05}O_{3-\delta}$ – ZnO (90-10 wt%) [9]	Symmetric pellet	1100		0.002 for 24h	(a) 20 vol% H_2/ 80 vol% He, 80 mL min^{-1} (b) 100 mL min^{-1} CO_2 and 120 mL min^{-1} N_2	Unstabe (CeO_2, $CeZn_5$ and Sr_2CeO_4 formation) verified by XRD, SEM and TEM	Not reported
$La_{5.5}WO_{11.25-d}$– $La_{0.87}Sr_{0.13}CrO_{3-\delta}$ 50-50 vol% [10]	Symmetric pellet	370-600	850	0.075 for 24h	(a) Wet 50 vol.% H_2 in He100 mL·min^{-1} for feed (b) Wet 15 vol.% CO_2 in Ar 150 mL·min^{-1}	Stable verified by TG analysis	Not reported
$BaCe_{0.65}Zr_{0.20}Y_{0.15}O_{3-\delta}$-$Ce_{0.8}Gd_{0.2}O_{2-\delta}$ 50-50 vol% [15]	Symmetric pellet	660	750	≈ 0.01 for 24h	(a) Wet 50% vol H_2 in He (100 mL·min^{-1}) (b) Wet 15 vol.% CO_2 in Ar 150 mL·min^{-1} for sweep	Stable verified by XRD, SEM and TG	Not reported
$BaCe_{0.65}Zr_{0.20}Y_{0.15}O_{3-\delta}$-$Ce_{0.8}Gd_{0.2}O_{2-\delta}$ 50-50 vol% THIS WORK	Asymmetric planar structure	19	750	≈ 0.08 for 100h	(a) Wet 50% vol H_2 in He (100 mL·min^{-1}) (b) Wet 15 vol.% CO_2 in Ar 135 mL·min^{-1} for sweep	Stable verified by XRD and SEM	Good mechanical stability in terms of flexural strength and hardness after operating cycle.
$BaCe_{0.8}Eu_{0.2}O_{3-\delta}$ - $Ce_{0.8}Y_{0.2}O_{2-\delta}$ 50-50 vol% [11]	Symmetric pellet	500	700	≈ 0.14 for 140h	(a) Wet 50 vol.% H_2 in He100 mL·min^{-1} for feed (b) Wet 15 vol.% CO_2 in Ar 150 mL·min^{-1} for sweep	Stable verified by XRD, SEM and TG	TEC evaluations in air. No cracks evaluated after thermochemical cycles

Conclusions

The influence of thermal aging treatments (100 h at the selected operating temperature of 750 °C) in different atmospheres (H_2, CO_2, H_2+CO_2) on the long-term microstructural and mechanical stability of BCZY-GDC membranes was deeply investigated. Either tape-cast asymmetric membranes (porous substrate supporting the dense active layer), or pellets (symmetric configuration) were considered.

The exposure of the membrane to H_2-atmosphere leads to lower flexural strength values, i.e. 22 MPa with respect to 70 MPa of the as-prepared membrane. This is caused by a general embrittlement of the asymmetric structure, due to chemical expansion/contraction of the GDC cell after the aging cycle. Indeed, micro-cracking of GDC grains is clearly observed in symmetric membranes. This phenomenon causes the decrease of GDC nano-hardness value from 12.8 (for the as-prepared membrane) to 8.8 GPa, impacting, therefore, the composite Vickers hardness value, i.e. 354 Hv with respect to 543 Hv of the as-prepared membrane.

The aging in CO_2 atmosphere causes a slightly increase in flexural strength values (81 MPa) due to the formation, especially in the porous support, of ZDC-$BaCO_3$ sub-micrometric phases at the expanse of the almost total amount of perovskite, strengthening the membrane microstructure. Higher hardness values (704 Hv) were also recorded due to the emerging of $BaCO_3$ islands on the symmetric membrane surface. It is worth to notice, however, that the carbonation reaction drastically affects the whole asymmetric membrane due to the open porous structure, while the BCZY-GDC pellets are only aged at the surface level, confirming the key-role of the membrane architecture.

The membrane aged for 100 h in the operating H_2+CO_2 atmosphere shows only a slight decrease in flexural strength and comparable hardness values because no evident morphological or structural changes (except the $BaCO_3$ formation in trace amount) were observed, regardless the membrane configuration.

Finally, promising and stable hydrogen permeation flux values were obtained on the asymmetric membrane at 750 °C, for 100 h, using wet 15 vol% CO_2 in Ar as sweep gas. Neither structural nor morphological modifications of the membrane were detected after the testing, confirming the results registered for the membrane aged in similar conditions (750 °C, H_2+CO_2 atmosphere). Further work is required to improve the catalytic activity of the support and minimize gas diffusion resistance through the porous media to implement the final hydrogen permeation. Nonetheless, the present results confirm the high potentiality of proton-ceramic membranes based on BCZY-GDC composite thanks to the encouraging hydrogen fluxes, microstructural and mechanical stability in operating atmospheres containing CO_2. This is therefore a further essential step towards the future industrialization of these systems in line with the objective defined by the "European Green Deal".

Conflicts of interest

There are no conflicts of interest to declare.

Acknowledgements

This work was financially supported by the agreement between the Italian Ministry of Economic Development and the Italian National Research Council ''Ricerca di sistema elettrico nazionale'' and by the Spanish Government (RTI2018-102161) and the Generalitat Valenciana (PROMETEO/2018/006).

References

[1] The European Green Deal: hydrogen is a priority area for a clean and circular economy | www.fch.europa.eu, (n.d.). https://www.fch.europa.eu/news/european-green-deal-hydrogen-priority-area-clean-and-circular-economy (accessed June 4, 2021).

[2] W. Deibert, M.E. Ivanova, S. Baumann, O. Guillon, W.A. Meulenberg, Ion-conducting ceramic membrane reactors for high-temperature applications, Journal of Membrane Science. 543 (2017) 79–97. https://doi.org/10.1016/j.memsci.2017.08.016.

[3] S.H. Morejudo, R. Zanón, S. Escolástico, I. Yuste-Tirados, H. Malerød-Fjeld, P.K. Vestre, W.G. Coors, A. Martínez, T. Norby, J.M. Serra, C. Kjølseth, Direct conversion of methane to aromatics in a catalytic co-ionic membrane reactor, Science. 353 (2016) 563–566. https://doi.org/10.1126/science.aag0274.

[4] H. Malerød-Fjeld, D. Clark, I. Yuste-Tirados, R. Zanón, D. Catalán-Martinez, D. Beeaff, S.H. Morejudo, P.K. Vestre, T. Norby, R. Haugsrud, J.M. Serra, C. Kjølseth, Thermo-electrochemical production of compressed hydrogen from methane with near-zero energy loss, Nat Energy. 2 (2017) 923–931. https://doi.org/10.1038/s41560-017-0029-4.

[5] N.A. Al-Mufachi, N.V. Rees, R. Steinberger-Wilkens, Hydrogen selective membranes: A review of palladium-based dense metal membranes, Renewable and Sustainable Energy Reviews. 47 (2015) 540–551. https://doi.org/10.1016/j.rser.2015.03.026.

[6] G. Bernardo, T. Araújo, T. da Silva Lopes, J. Sousa, A. Mendes, Recent advances in membrane technologies for hydrogen purification, International Journal of Hydrogen Energy. 45 (2020) 7313–7338. https://doi.org/10.1016/j.ijhydene.2019.06.162.

[7] S.S. Hashim, M.R. Somalu, K.S. Loh, S. Liu, W. Zhou, J. Sunarso, Perovskite-based proton conducting membranes for hydrogen separation: A review, International Journal of Hydrogen Energy. 43 (2018) 15281–15305. https://doi.org/10.1016/j.ijhydene.2018.06.045.

[8] H. Wang, X. Wang, B. Meng, X. Tan, K.S. Loh, J. Sunarso, S. Liu, Perovskite-based mixed protonic–electronic conducting membranes for hydrogen separation: Recent status and advances, Journal of Industrial and Engineering Chemistry. 60 (2018) 297–306. https://doi.org/10.1016/j.jiec.2017.11.016.

[9] T. Wang, H. Zhang, B. Meng, X. Wang, J. Sunarso, X. Tan, S. Liu, $SrCe_{0.95}Y_{0.05}O_{3-\delta}$–ZnO dual-phase membranes for hydrogen permeation, RSC Adv. 6 (2016) 36786–36793. https://doi.org/10.1039/C6RA02921C.

[10] S. Escolástico, C. Solís, C. Kjølseth, J.M. Serra, Outstanding hydrogen permeation through CO_2-stable dual-phase ceramic membranes, Energy Environ. Sci. 7 (2014) 3736–3746. https://doi.org/10.1039/C4EE02066A.

[11] M.E. Ivanova, S. Escolástico, M. Balaguer, J. Palisaitis, Y.J. Sohn, W.A. Meulenberg, O. Guillon, J. Mayer, J.M. Serra, Hydrogen separation through tailored dual phase membranes with nominal composition $BaCe_{0.8}Eu_{0.2}O_{3-\delta}$:$Ce_{0.8}Y_{0.2}O_{2-\delta}$ at intermediate temperatures, Sci Rep. 6 (2016) 34773. https://doi.org/10.1038/srep34773.

[12] J.M. Polfus, W. Xing, M.-L. Fontaine, C. Denonville, P.P. Henriksen, R. Bredesen, Hydrogen separation membranes based on dense ceramic composites in the $La_{27}W_5O_{55.5}$–$LaCrO_3$ system, Journal of Membrane Science. 479 (2015) 39–45. https://doi.org/10.1016/j.memsci.2015.01.027.

[13] J. S. Fish, S. Ricote, R. O'Hayre, N. Bonanos, Electrical properties and flux performance of composite ceramic hydrogen separation membranes, Journal of Materials Chemistry A. 3 (2015) 5392–5401. https://doi.org/10.1039/C5TA00450K.

[14] D. Montaleone, E. Mercadelli, S. Escolástico, A. Gondolini, J.M. Serra, A. Sanson, All-ceramic asymmetric membranes with superior hydrogen permeation, J. Mater. Chem. A. 6 (2018) 15718–15727. https://doi.org/10.1039/C8TA04764B.

[15] E. Rebollo, C. Mortalò, S. Escolástico, S. Boldrini, S. Barison, J.M. Serra, M. Fabrizio, Exceptional hydrogen permeation of all-ceramic composite robust membranes based on

$BaCe_{0.65}Zr_{0.20}Y_{0.15}O_{3-\delta}$ and Y- or Gd-doped ceria, Energy Environ. Sci. 8 (2015) 3675–3686. https://doi.org/10.1039/C5EE01793A.

[16] C. Mortalò, E. Rebollo, S. Escolástico, S. Deambrosis, K. Haas-Santo, M. Rancan, R. Dittmeyer, L. Armelao, M. Fabrizio, Enhanced sulfur tolerance of $BaCe_{0.65}Zr_{0.20}Y_{0.15}O_{3-\delta}$-$Ce_{0.85}Gd_{0.15}O_{2-\delta}$ composite for hydrogen separation membranes, Journal of Membrane Science. 564 (2018) 123–132. https://doi.org/10.1016/j.memsci.2018.07.015.

[17] D. Montaleone, E. Mercadelli, A. Gondolini, P. Pinasco, A. Sanson, On the compatibility of dual phase $BaCe_{0.65}Zr_{0.2}Y_{0.15}O_3$-based membrane for hydrogen separation application, Ceramics International. 43 (2017) 10151–10157. https://doi.org/10.1016/j.ceramint.2017.05.039.

[18] E. Mercadelli, D. Montaleone, A. Gondolini, P. Pinasco, A. Sanson, Tape-cast asymmetric membranes for hydrogen separation, Ceramics International. 43 (2017) 8010–8017. https://doi.org/10.1016/j.ceramint.2017.03.099.

[19] D. Montaleone, E. Mercadelli, A. Gondolini, M. Ardit, P. Pinasco, A. Sanson, Role of the sintering atmosphere in the densification and phase composition of asymmetric BCZY-GDC composite membrane, Journal of the European Ceramic Society. 39 (2019) 21–29. https://doi.org/10.1016/j.jeurceramsoc.2018.01.043.

[20] E. Mercadelli, A. Gondolini, D. Montaleone, P. Pinasco, S. Escolástico, J.M. Serra, A. Sanson, Production strategies of asymmetric $BaCe_{0.65}Zr_{0.20}Y_{0.15}O_{3-\delta}$ – $Ce_{0.8}Gd_{0.2}O_{2-\delta}$ membrane for hydrogen separation, International Journal of Hydrogen Energy. 45 (2020) 7468–7478. https://doi.org/10.1016/j.ijhydene.2019.03.148.

[21] E. Mercadelli, A. Gondolini, D. Montaleone, P. Pinasco, A. Sanson, Innovative strategy for designing proton conducting ceramic tapes and multilayers for energy applications, Journal of the European Ceramic Society. 41 (2021) 488–496. https://doi.org/10.1016/j.jeurceramsoc.2020.09.016.

[22] C. Mortalò, A. Santoru, C. Pistidda, E. Rebollo, M. Boaro, C. Leonelli, M. Fabrizio, Structural evolution of $BaCe_{0.65}Zr_{0.20}Y_{0.15}O_{3-\delta}$-$Ce_{0.85}Gd_{0.15}O_{2-\delta}$ composite MPEC membrane by in-situ synchrotron XRD analyses, Materials Today Energy. 13 (2019) 331–341. https://doi.org/10.1016/j.mtener.2019.06.004.

[23] J. Malzbender, Mechanical aspects of ceramic membrane materials, Ceramics International. 42 (2016) 7899–7911. https://doi.org/10.1016/j.ceramint.2016.02.136.

[24] L. Chen, L. Liu, J. Xue, L. Zhuang, H. Wang, Asymmetric membrane structure: An efficient approach to enhance hydrogen separation performance, Separation and Purification Technology. 207 (2018) 363–369. https://doi.org/10.1016/j.seppur.2018.06.066.

[25] G. Pećanac, S. Baumann, J. Malzbender, Mechanical properties and lifetime predictions for $Ba_{0.5}Sr_{0.5}Co_{0.8}Fe_{0.2}O_{3-\delta}$ membrane material, Journal of Membrane Science. 385–386 (2011) 263–268. https://doi.org/10.1016/j.memsci.2011.10.005.

[26] G. Pećanac, S. Foghmoes, M. Lipińska-Chwałek, S. Baumann, T. Beck, J. Malzbender, Strength degradation and failure limits of dense and porous ceramic membrane materials, Journal of the European Ceramic Society. 33 (2013) 2689–2698. https://doi.org/10.1016/j.jeurceramsoc.2013.04.018.

[27] M. Lipińska-Chwałek, G. Pećanac, J. Malzbender, Creep behaviour of membrane and substrate materials for oxygen separation units, Journal of the European Ceramic Society. 33 (2013) 1841–1848. https://doi.org/10.1016/j.jeurceramsoc.2013.02.007.

[28] V.K. Stournari, Thermo-mechanical Properties of Mixed Ionic-Electronic Conducting Membranes for Gas Separation, Forschungszentrum Jülich GmbH Zentralbibliothek, Verlag, 2016. https://juser.fz-juelich.de/record/283575 (accessed August 23, 2021).

[29] V. Stournari, W. Deibert, M.E. Ivanova, C. Krautgasser, R. Bermejo, J. Malzbender, Mechanical properties of tape casted Lanthanum Tungstate for membrane substrate application, Ceramics International. 42 (2016) 15177–15182. https://doi.org/10.1016/j.ceramint.2016.06.109.

[30] W. Deibert, V. Stournari, M.E. Ivanova, S. Escolástico, J.M. Serra, J. Malzbender, T. Beck, L. Singheiser, O. Guillon, W.A. Meulenberg, Effect of microstructure on electrical and mechanical properties of $La_{5.4}WO_{12-\delta}$ proton conductor, Journal of the European Ceramic Society. 38 (2018) 3527–3538. https://doi.org/10.1016/j.jeurceramsoc.2018.04.009.

[31] S. Escolástico, V. Stournari, J. Malzbender, K. Haas-Santo, R. Dittmeyer, J.M. Serra, Chemical stability in H_2S and creep characterization of the mixed protonic conductor $Nd_{5.5}WO_{11.25-\delta}$, (2018). https://doi.org/10.1016/J.IJHYDENE.2018.03.060.

[32] Y. Guo, Y. Lin, R. Ran, Z. Shao, Zirconium doping effect on the performance of proton-conducting $BaZr_yCe_{0.8-y}Y_{0.2}O_{3-\delta}$ ($0.0\leq y\leq 0.8$) for fuel cell applications, Journal of Power Sources. 193 (2009) 400–407. https://doi.org/10.1016/j.jpowsour.2009.03.044.

[33] M.F. Bekheet, M. Grünbacher, L. Schlicker, A. Gili, A. Doran, J.D. Epping, A. Gurlo, B. Klötzer, S. Penner, On the structural stability of crystalline ceria phases in undoped and acceptor-doped ceria materials under in situ reduction conditions, CrystEngComm. 21 (2018) 145–154. https://doi.org/10.1039/C8CE01726C.

[34] D. Medvedev, J. Lyagaeva, S. Plaksin, A. Demin, P. Tsiakaras, Sulfur and carbon tolerance of $BaCeO_3$–$BaZrO_3$ proton-conducting materials, Journal of Power Sources. 273 (2015) 716–723. https://doi.org/10.1016/j.jpowsour.2014.09.116.

[35] H. Cheng, B. Meng, X. Wang, X. Meng, S. Liu, CO_2 and Steam-Assisted H_2 Separation through $BaCe_{0.8}Y_{0.2}O_{3-\delta}$–$Ce_{0.8}Y_{0.2}O_{2-\delta}$ Hollow Fiber Membranes, Energy Fuels. 34 (2020) 683–689. https://doi.org/10.1021/acs.energyfuels.9b02972.

[36] A.K.E. Andersson, S.M. Selbach, C.S. Knee, T. Grande, Chemical Expansion Due to Hydration of Proton-Conducting Perovskite Oxide Ceramics, J. Am. Ceram. Soc. 97 (2014) 2654–2661. https://doi.org/10.1111/jace.12990.

[37] G. Hudish, A. Manerbino, W.G. Coors, S. Ricote, Chemical expansion in $BaZr_{0.9-x}Ce_xY_{0.1}O_{3-\delta}$ ($x = 0$ and 0.2) upon hydration determined by high-temperature X-ray diffraction, Journal of the American Ceramic Society. 101 (2018) 1298–1309. https://doi.org/10.1111/jace.15275.

[38] M. Morales, J.J. Roa, X.G. Capdevila, M. Segarra, S. Piñol, Mechanical properties at the nanometer scale of GDC and YSZ used as electrolytes for solid oxide fuel cells, Acta Materialia. 58 (2010) 2504–2509. https://doi.org/10.1016/j.actamat.2009.12.036.

[39] P.-F. Yang, D.-L. Chen, S.-R. Jian, S.-W. Lee, C.-J. Tseng, Mechanical Properties of $Ba_{1-x}K_xCe_{0.6}Zr_{0.2}Y_{0.2}O_{3-\delta}$ Oxides by Nanoindentation, Procedia Engineering. 79 (2014) 599–605. https://doi.org/10.1016/j.proeng.2014.06.385.

[40] W. Zhou, J. Malzbender, F. Zeng, W. Deibert, O. Guillon, R. Schwaiger, W.A. Meulenberg, Mechanical properties of $BaCe_{0.65}Zr_{0.2}Y_{0.15}O_{3-\delta}$ proton-conducting material determined using different nanoindentation methods, Journal of the European Ceramic Society. 40 (2020) 5653–5661. https://doi.org/10.1016/j.jeurceramsoc.2020.07.044.

[41] K. Sato, M. Nishioka, H. Higashi, T. Inoue, Y. Hasegawa, Y. Wakui, T.M. Suzuki, S. Hamakawa, Influence of CO_2 and H_2O on the separation of hydrogen over two types of Pd membranes: Thin metal membrane and pore-filling-type membrane, Journal of Membrane Science. 415–416 (2012) 85–92. https://doi.org/10.1016/j.memsci.2012.04.053.

[42] Z. Wang, N. Dewangan, S. Das, M.H. Wai, S. Kawi, High oxygen permeable and CO_2-tolerant $SrCo_xFe_{0.9-x}Nb_{0.1}O_{3-\delta}$ ($x = 0.1$–0.8) perovskite membranes: Behavior and mechanism, Separation and Purification Technology. 201 (2018) 30–40. https://doi.org/10.1016/j.seppur.2018.02.046.

[43] U. (Balu) Balachandran, T.H. Lee, C.Y. Park, J.E. Emerson, J.J. Picciolo, S.E. Dorris, Dense cermet membranes for hydrogen separation, Separation and Purification Technology. 121 (2014) 54–59. https://doi.org/10.1016/j.seppur.2013.10.001.

[44] C. Zuo, T.H. Lee, S.E. Dorris, U. Balachandran, M. Liu, Composite Ni–$Ba(Zr_{0.1}Ce_{0.7}Y_{0.2})O_3$ membrane for hydrogen separation, Journal of Power Sources. 159 (2006) 1291–1295. https://doi.org/10.1016/j.jpowsour.2005.12.042.

[45] C. Zuo, S.E. Dorris, U. Balachandran, M. Liu, Effect of Zr-Doping on the Chemical Stability and Hydrogen Permeation of the Ni−$BaCe_{0.8}Y_{0.2}O_{3-\alpha}$ Mixed Protonic−Electronic Conductor, Chem. Mater. 18 (2006) 4647–4650. https://doi.org/10.1021/cm0518224.

[46] S. Fang, K.S. Brinkman, F. Chen, Hydrogen permeability and chemical stability of Ni–$BaZr_{0.1}Ce_{0.7}Y_{0.1}Yb_{0.1}O_{3-\delta}$ membrane in concentrated H_2O and CO_2, Journal of Membrane Science. 467 (2014) 85–92. https://doi.org/10.1016/j.memsci.2014.05.008.

[47] Z. Zhu, W. Sun, Y. Dong, Z. Wang, Z. Shi, Q. Zhang, W. Liu, Evaluation of hydrogen permeation properties of Ni–$Ba(Zr_{0.7}Pr_{0.1}Y_{0.2})O_{3-\delta}$ cermet membranes, International Journal of Hydrogen Energy. 39 (2014) 11683–11689. https://doi.org/10.1016/j.ijhydene.2014.05.163.

[48] Y. Shang, L. Wei, X. Meng, B. Meng, N. Yang, J. Sunarso, S. Liu, CO_2-enhanced hydrogen permeability of dual-layered A-site deficient $Ba_{0.95}Ce_{0.85}Tb_{0.05}Zr_{0.1}O_{3-\delta}$-based hollow fiber membrane, Journal of Membrane Science. 546 (2018) 82–89. https://doi.org/10.1016/j.memsci.2017.10.012.

[49] H. Cheng, X. Wang, X. Meng, B. Meng, J. Sunarso, X. Tan, L. Liu, S. Liu, Dual-layer $BaCe_{0.8}Y_{0.2}O_{3-\delta}$-$Ce_{0.8}Y_{0.2}O_{2-\delta}$/$BaCe_{0.8}Y_{0.2}O_{3-\delta}$-Ni hollow fiber membranes for H_2 separation, Journal of Membrane Science. 601 (2020) 117801. https://doi.org/10.1016/j.memsci.2019.117801.